Application of Polynomial Chaos to Quantify Uncertainty in Deterministic Channel Models

Andrew C. M. Austin, *Member, IEEE*, Neeraj Sood *Student Member, IEEE*, Joseph Siu, and Costas D. Sarris, *Senior Member, IEEE*

***Abstract*—A non-intrusive formulation of the polynomial chaos method is applied to quantify the uncertainties in deterministic models of the indoor radio channel. Deterministic models based on the Finite-Difference Time-Domain (FDTD) method and ray tracing are examined. Various sources of parameter uncertainty are considered, including randomness in the material properties, building geometry, and the spatial location of transmitting and receiving antennas. The polynomial chaos results are confirmed against Monte Carlo simulations and experimental measurements. The analysis shows the expected variation in the sector-averaged path loss can be considerable for relatively small input parameter uncertainties, leading to the conclusion that a single simulation run using 'nominal values' may be insufficient to adequately characterize the indoor radio channel.**

I. Introduction

UNDERSTANDING the propagation characteristics of the radio channel is essential to predict the performance of modern wireless systems operating in outdoor environments and within buildings [1]. Consequently there has been increased interest in developing site-specific models for indoor environments using deterministic methods with a rigorous electromagnetic basis. For example, ray-tracing (e.g. [2], [3]) and time-domain methods (e.g. [4]–[7]) have been applied to model radio wave propagation within buildings. Most deterministic models require a detailed characterization of the internal environment, particularly the geometry and corresponding dielectric properties.

However, considerable uncertainty can exist in the description of the environment. The dielectric properties of typical building materials are difficult to measure *in situ*, and nominal values from tabulated experimental data (e.g. [8], [9]) are often used [3], [7]. Changes in the atmospheric moisture content, variability in the manufacturing processes, or other random factors will introduce uncertainty in the values of the relative permittivity and electrical conductivity. Uncertainty in the geometry can arise as detailed floor plans are usually not available for older buildings, and must be reconstructed from physical measurements, or converted from blue-prints. Furthermore, even if detailed architectural drawings are available, uncertainty often remains as construction tolerances and later modifications may not be recorded. The uncertainty in the materials and building layout can be expressed as random variables—characterized by appropriate probability density functions (PDFs)—with the actual geometry and dielectric properties viewed as a particular realization [10, pp. 1–3]. The randomness in the input parameters 'propagates' through the deterministic channel models and introduces uncertainty in the results [11, pp. 6–7]. The size of this output uncertainty is related to the uncertainties in the input and how these interact with the model. A single simulation run (at the nominal values or otherwise) does not account for the uncertainties, which can typically only be examined by collating multiple results.

Previous investigations have shown ray-tracing or FDTD models of the radio channel can be highly dependent on the building geometry and dielectric properties [3], [4], [7]. For example, Wang *et. al*, and later Athanasiadou *et. al*, identified many of the key factors influencing the sensitivity of outdoor ray-tracing models [12], [13]. However, these findings were based on sweeping each parameter over a range of values to fit the simulated results against measurements. This paper focuses on the inverse problem, namely "what is the expected variation in the predictions when the inputs are uncertain?". While this problem has not been examined in detail for either FDTD or ray-tracing models of the indoor channel, such an analysis is important to assess the sensitivity of the predictions and can give a measure of confidence in the simulated results. This is particularly relevant when using such models to plan or optimize wireless system deployments, where no (or limited) experimental data is available.

The Monte Carlo method is widely used to quantify the impacts of uncertainty and randomness in numerical models with multiple inputs, as the size of the parameter space increases exponentially with the number of independent random variables considered; e.g. for N independent inputs the parameter space spans N dimensions, and cannot be fully explored by considering each input independently. In the Monte Carlo method a large number of random inputs are generated based on prescribed (or assumed) probability distributions, and the model is solved for each realization. Statistical information, such as the mean and variance are found by appropriately collating the random solutions [11, pp. 8–9]. The Monte Carlo method has been demonstrated to provide accurate results for electromagnetic problems [14]. However, the slow rate of convergence generally limits its applicability for computationally large problems, such as deterministic channel modelling. For example, the mean value converges as $\frac{1}{\sqrt{M}}$, where M is the number of realizations [11, pp. 8–9]. Despite the computational limitations, the Monte Carlo method

Manuscript received January 1, 1900; revised January 2, 1900; accepted January 3, 1900. Colour versions of the figures are available online.

A.C.M. Austin, N. Sood and C.D. Sarris are with Edward S. Rogers Sr. Department of Electrical and Computer Engineering, University of Toronto, Toronto, ON, M5S 3G4, Canada (e-mail: acm.austin@ieee.org).

J. Siu is with Thales Canada Transportation Solutions, Toronto, ON, Canada.

remains widely used as it is simple to apply and convergence is independent of dimensionality [11, p. 9]. Other methods, such as perturbation can also be used for sensitivity and uncertainty analysis. However, perturbation is usually only valid for small changes in the inputs.

More recently, methods based on generalized polynomial chaos—an extension of the homogeneous chaos introduced by Wiener [15]—have been developed to quantify uncertainty in numerical models [10], [16]. The polynomial chaos method approximates quantities in a stochastic process as the finite summation of orthogonal basis polynomials in the random input parameter space. The resulting polynomial expansion thus provides a surrogate model for the underlying system, i.e. an accurate, but relatively simple expression relating the outputs of interest to the input parameters. Statistics computed from the surrogate model will be a good approximation to the statistics of the real system. The polynomial chaos method converges significantly faster than the Monte Carlo method, however, the computational efficiency depends on the number of random inputs and order of the polynomial expansion [16]. Polynomial chaos has previously been applied to quantify uncertainties in computational electromagnetic problems [17], including the variability in specific absorption rate caused random handset position and orientation [18], [19].

A brief overview of polynomial chaos theory is outlined in section II, discussing efficient methods to evaluate coefficients in the expansion using sparse grids and quantifying global sensitivity. Section III outlines the FDTD channel models and discusses how polynomial chaos techniques can be applied to estimate the uncertainty due to material properties and building geometry. Section IV quantifies the uncertainty introduced by randomness in the material properties and locations of the transmitting and receiving antennas for a ray-tracing channel model.

II. Formulation

A. The Polynomial Chaos Expansion

The polynomial chaos expansion (PCE) uses orthogonal basis polynomials to approximate the functional form between a stochastic quantity of interest and each of the random inputs [16]. A stochastic quantity, R, can be expressed as the truncated series expansion

$$R(\boldsymbol{\xi}) = \sum_{j=0}^{P} a_j \Psi_j(\boldsymbol{\xi}), \tag{1}$$

where a_j is the weighting coefficient for the generalized polynomial chaos basis, $\Psi_j(\cdot)$, in the N input variables, $\boldsymbol{\xi} = \{\xi_1, \xi_2, \ldots\ \xi_N\}$. The number of terms is given by $P+1 = \frac{(N+D)!}{N!D!}$, where D is the highest polynomial order in the expansion [16]. The construction of the multi-variate basis functions, $\Psi_j(\boldsymbol{\xi})$ is outlined in appendix A. Eqn. (1) can be applied to characterize the uncertainty in numerical models by expanding either the governing equations, or the solution in terms of the random inputs; these approaches are termed *intrusive* and *non-intrusive* respectively [11]. This paper focuses on the non-intrusive approach, as the implementation of intrusive polynomial chaos generally requires considerably more computational resources to solve than the non-stochastic problem [20]. For example an FDTD implementation of the PCE increases the total memory consumption and run time by factor $P+1$ [17]. For computationally large problems, such as indoor propagation, an intrusive formulation is not currently feasible.

B. Numerical Evaluation of PCE Coefficients

The polynomial chaos basis functions, $\Psi_i(\boldsymbol{\xi})$, are orthogonal with respect to a probability measure, e.g.

$$\begin{aligned}\langle \Psi_i(\boldsymbol{\xi}), \Psi_j(\boldsymbol{\xi}) \rangle &= \int \Psi_i(\boldsymbol{\xi}) \Psi_j(\boldsymbol{\xi}) \rho(\boldsymbol{\xi})\, \mathrm{d}\boldsymbol{\xi} \\ &= \left\langle \Psi_j^2(\boldsymbol{\xi}) \right\rangle \delta_{i,j},\end{aligned} \tag{2}$$

where $\delta_{i,j}$ is the Kronecker delta function, and $\rho(\boldsymbol{\xi})$ is the probability weighting function. The input variables are assumed to be independent as the weighting function is defined $\rho(\boldsymbol{\xi}) = \prod_{i=1}^{N} \rho(\xi_i)$, where $\rho(\xi_i)$ is the PDF of the i-th input variable [16]. Using the orthogonality condition (2), the coefficients, a_j in (1), can be found by projection

$$\begin{aligned}a_j &= \frac{\langle R(\boldsymbol{\xi}), \Psi_j(\boldsymbol{\xi}) \rangle}{\left\langle \Psi_j^2(\boldsymbol{\xi}) \right\rangle} \\ &= \frac{1}{\left\langle \Psi_j^2(\boldsymbol{\xi}) \right\rangle} \int_{\Omega^N} R(\boldsymbol{\xi})\, \Psi_j(\boldsymbol{\xi})\, \rho(\boldsymbol{\xi})\, \mathrm{d}\boldsymbol{\xi},\end{aligned} \tag{3}$$

where the integration is over the N-dimensional input parameter space, Ω^N. The multi-dimensional integration in (3) can be evaluated using numerical quadrature, e.g.

$$\begin{aligned}&\int_{\Omega^N} R(\boldsymbol{\xi})\, \Psi_j(\boldsymbol{\xi})\, \rho(\boldsymbol{\xi})\, \mathrm{d}\boldsymbol{\xi} \\ &\qquad \approx \sum_q R\left(\boldsymbol{\xi}^{\{q\}}\right) \Psi_j\left(\boldsymbol{\xi}^{\{q\}}\right) w^{\{q\}},\end{aligned} \tag{4}$$

where $\boldsymbol{\xi}^{\{q\}}$ and $w^{\{q\}}$ are the integration quadrature points and weights respectively. The coefficients in (1) are thus evaluated by collating the results from $\{q\}$ simulations with inputs $\boldsymbol{\xi}^{\{q\}}$. In the general case with multiple inputs (4) requires forming a N-dimensional tensor-product grid of efficient one-dimensional integration rules [20]. In this paper one-dimensional Gaussian [21] and Kronrod-Patterson (KP) [22] quadrature rules are used. However the number of quadrature points to accurately estimate the integral rises exponentially with N and D. To reduce the computational costs sparse-grid integration techniques based on the Smolyak algorithm are applied [20]. In many cases these can accurately approximate multi-dimensional integrals with substantially fewer quadrature points [22]. The construction of the Smolyak grids from the one-dimensional quadrature rules is detailed in appendix B.

C. Estimating Statistics from the PCE

The mean and variance of the output, R, can be found from the coefficients of (1) [11, p. 39],

$$\mu[R(\boldsymbol{\xi})] = a_0, \tag{5}$$

$$\sigma^2[R(\boldsymbol{\xi})] = \sum_{j=1}^{P} a_j^2 \left\langle \Psi_j^2\left(\boldsymbol{\xi}\right) \right\rangle. \tag{6}$$

In general the PCE will contain a large number of terms, and consequently it is difficult to analytically determine the PDF of $R(\boldsymbol{\xi})$. However, the PDF can be estimated by running a Monte Carlo analysis on (1). The computational cost is relatively low as this expression only contains polynomial terms.

The global sensitivity of $R(\boldsymbol{\xi})$ to the various input parameter uncertainties can be found by applying the the Sobol decomposition to (1) [23]. The Sobol decomposition yields a set of conditional variances—termed the Sobol indices—indicating the relative contribution each combination of input parameters makes toward to uncertainty in R. The Sobol indices for the set of inputs u are given by [23]

$$S_u = \frac{\sum_{k \in K_u} a_k^2 \left\langle \Psi_k^2 \left(\boldsymbol{\xi} \right) \right\rangle}{\sigma^2 \left[R(\boldsymbol{\xi}) \right]}, \tag{7}$$

where K_u is an index to the expansion terms in (1) that contain u. For N input variables (7) yields $2^N - 1$ indices, and in practice it is more useful to sum S_u for each input variable ξ_i; these are termed the total indices,

$$S_{T_i} = \sum_{u \ni i} S_u \tag{8}$$

and represents the sensitivity in R due to ξ_i alone and all its interactions with the other variables.

III. Uncertainty in FDTD Channel Models

The non-intrusive polynomial-chaos technique is now applied to examine uncertainty in FDTD models of the indoor radio channel. It is important to distinguish between the outputs of the channel models (which are often characterized statistically due to the complexity of the propagation processes, e.g. Rayleigh/Rician and Lognormal models for the instantaneous received power), and the variations introduced by uncertainty in the material properties or other inputs. The results presented in this paper focus on characterizing the latter. The uncertainty in the material properties and the building geometry are considered separately to reduce the size of the parameter space, and to ensure results from the polynomial chaos method can be validated against Monte Carlo simulations. Similarly, two-dimensional FDTD simulations are used to limit the computational costs for the Monte-Carlo analysis. Previous findings indicate many of the dominant propagation mechanisms identified in a three-dimensional analysis are present on two-dimensional 'slices' through the geometry [7].

A. Uncertainty in the Material Properties

A two-dimensional TM_z implementation of the FDTD method is used to examine propagation on a simplified horizontal 'slice' through a multi-storey office building. Fig 1(a) shows the floor plan: a 0.30 m thick concrete services shaft (containing elevators and stairwells) is located in the centre of the floor; the remaining space is divided into corridors and offices by 0.10 m thick drywall partitions; and 1 cm thick glass windows surround the outside face of the building. The walls are modelled in the FDTD mesh as uniformly homogeneous dielectric slabs with appropriate material properties. The nominal values and uncertainties in the material properties are listed in Table I (uncertainty in the glass conductivity was not considered to reduce the size of the parameter space). In the absence of detailed information for the expected variations, the material properties are assumed to follow uniform distributions, with limits $\pm 20\%$ about their nominal values [9]. It is also assumed that the randomness in each material property is independent. The polynomial chaos expansion is truncated at total order $D = \{2, 3, 4\}$. Increasing D improves the accuracy, but requires additional simulations to evaluate the inner products [20]. The number of quadrature points required for Smolyak sparse grids generated using Gauss-Legendre integration rules are 61, 241 and 781 respectively.

TABLE I
Material Properties and Associated Uncertainty

	Nominal Values		Distribution	Uncertainty	
	ϵ_r	σ_E (mS/m)		ϵ_r	σ_E (mS/m)
Concrete	5.0	50.0	Uniform	4.0–6.0	40.0–60.0
Drywall	3.0	12.0	Uniform	2.4–3.6	9.6–14.4
Glass	3.0	4.0	Uniform	2.4–3.6	—

A single E_z field component, located at a point indicated with '$\times$' in Fig. 1(a), is used to excite the FDTD lattice with a 1.0 GHz modulated Gaussian pulse. Square lattice cells, with $\Delta = 0.01$ m are used, and the time-step is set at 0.99 of the Courant limit. The FDTD simulation domain is 18 m$\times 18$ m and is terminated with a 12-cell thick UPML [24]. Each simulation was run for 12,000 time steps and the 1.0 GHz electric field magnitude and phase were extracted by multiplying the time-series with a 1.0 GHz cisoid. The resulting steady-state E_z fields are converted to path loss by normalizing the source to $1\angle 0$ and averaged over $3\lambda \times 3\lambda$ sectors to remove the effects of multipath fading [7], [25], PL (dB) $= -20 \log_{10} \left(E_{\text{sector avg.}} \right)$. The path loss (in dB units) for each sector is then approximated as a function of the material properties using (1), with (3) and (4) used to find the coefficients. The uncertainty can then be quantified by computing statistics such as the PDFs, mean, and 95% confidence intervals (CI) [17], i.e. 95% of the variation in received power for each sector can be expected to fall within the range indicated.

Uncertainty in ϵ_r introduces randomness in the strength of the reflected (or transmitted) components; similarly, uncertainty in σ_E affects the attenuation of penetrating components. Although the actual dependence of the path loss to the variations in material properties is governed by Maxwell's Equations, an accurate polynomial approximation can be derived using polynomial chaos expansion, (1). Fig. 2(a) and (b) show PDFs of the sector-averaged path loss computed using polynomial chaos expansions (truncated at total order $D = 2$–4) compared against those computed from 2000 Monte Carlo trials of the FDTD channel model. As indicated in Fig. 1(b), the two sectors are centred at $x = 5$ m, $y = 5$ m (where the LOS path dominates), and $x = 2$ m, $y = 16$ m (in the radio shadow of the services shaft). For both sectors, statistics (mean and standard deviation) computed using the polynomial chaos results compare well with the Monte-Carlo

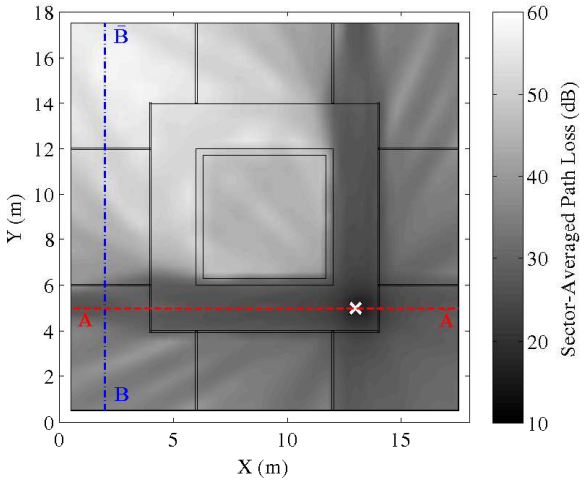

(a)

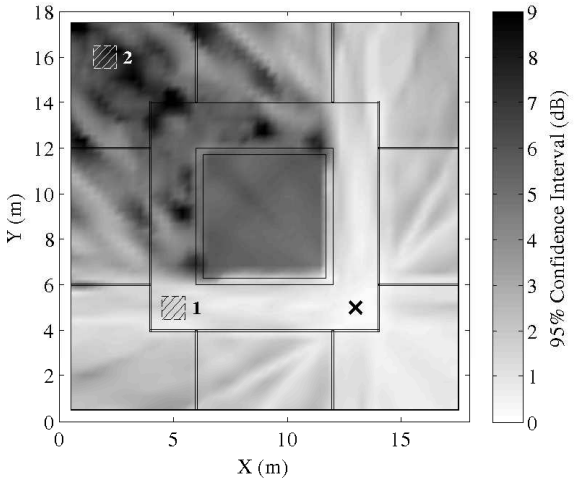

(b)

Fig. 1. Statistics of the sector-averaged path loss due to uncertainty in the material parameters: (a) Spatial variation of the mean path loss; and (b) Contour plot of the 95% confidence interval. The location of the sectors used to compute the PDFs are indicated.

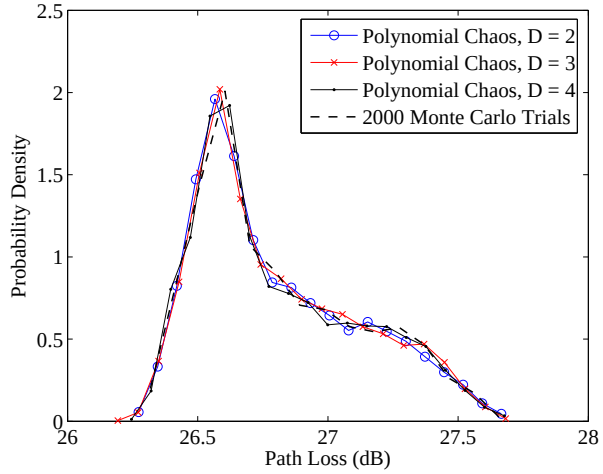

(a)

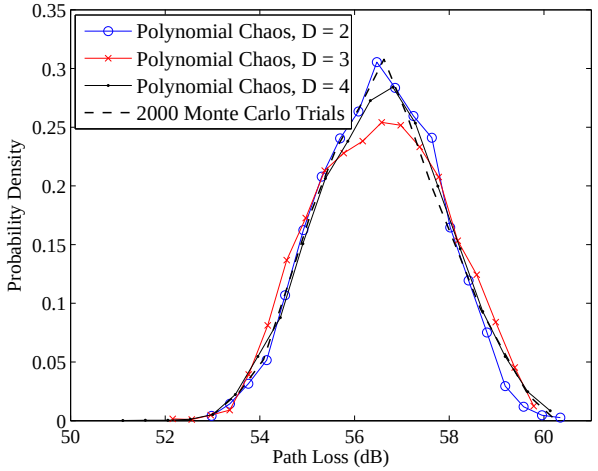

(b)

Fig. 2. Probability distributions of the sector-averaged path loss due to uncertainty in the material properties, as detailed in Table I, computed using polynomial chaos and Monte-Carlo—(a) sector 1 centred at $x = 5$ m, $y = 5$ m; and (b) sector 2 centred at $x = 2$ m, $y = 16$ m.

simulations, and similar observations can be made for the other sectors. Truncating the polynomial chaos expansion at $D = 2$ is sufficient to characterize the uncertainty in sector 1, and increasing the order of the expansion does not improve the results relative to the Monte-Carlo simulations. For sector 2, the $D = 2$ expansion agrees well at the peak, however in the tails of the PDF, particularly between 57–60 dB there is divergence away from the MC results. The PCE is a global interpolation, so in this case $D = 3$ improves convergence in the tails, at the expense of the peak, while the $D = 4$ truncation achieves a good agreement in both the tails and the peak of the PDF. However, both these effects are relatively small, and the $D = 2$ expansion would be adequate for most practical cases, resulting in a 30-fold decrease in computational costs relative to the Monte Carlo simulations. For example, each FDTD simulation takes approximately 20 minutes to complete: 2000 Monte-Carlo trials thus require 28 days of computer-time; whereas 61 polynomial chaos simulations take 20 hours.

Fig. 1(a) and (b) show the FDTD-simulated path loss and the associated uncertainty in these results due to randomness in the material properties (as listed in Table I). The polynomial chaos expansion is truncated at $D = 3$. The path loss generally increases with distance away from the transmitter. The attenuation introduced by propagation through drywall partitions increases path loss in the offices, relative to values observed in the corridors—where strong line-of-sight (LOS) paths exist. The concrete services shaft casts a large radio shadow across the floor, significantly reducing the power in regions opposite the transmitter (the path loss within the shaft is also high).

The results in Fig. 1(b) show path loss uncertainty is low in regions close to the transmitting antenna, but increases when propagating through the drywall partitions (1–2 dB) or into the services shaft (3–5 dB). Furthermore, as shown in Fig. 3(a), the 95% CI on LOS paths ($\mathbf{A}\bar{\mathbf{A}}$) remains small—in most cases below 1.0 dB—and could be safely ignored

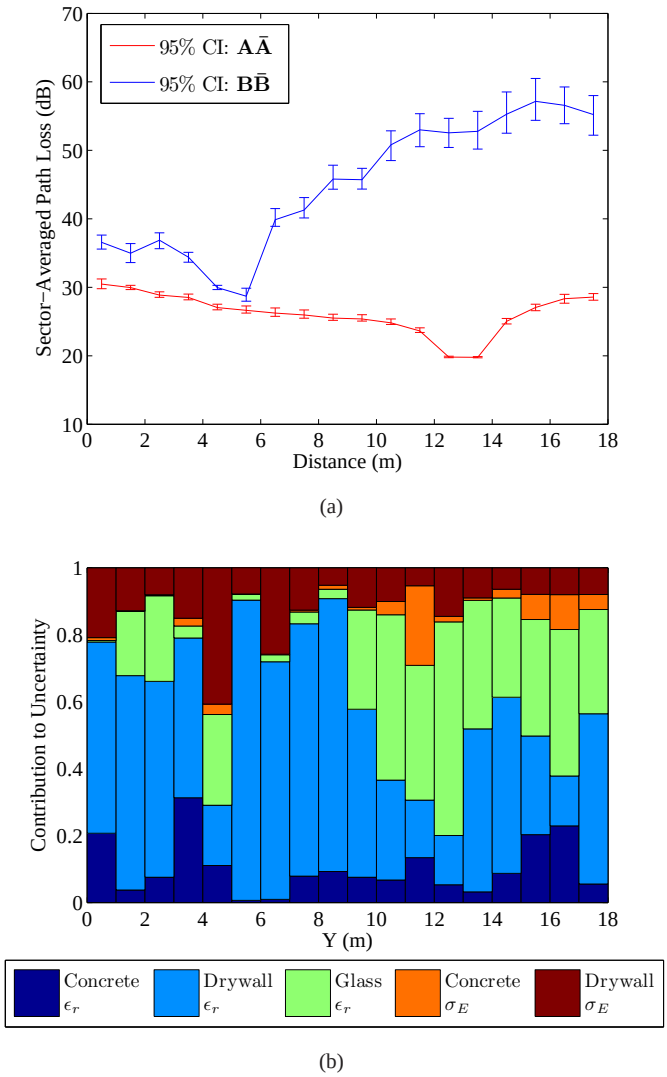

Fig. 3. (a) Mean power and 95% confidence limits on $\mathbf{A\bar{A}}$ and $\mathbf{B\bar{B}}$; and (b) Relative contribution of each material property to the uncertainty observed on $\mathbf{B\bar{B}}$.

for most practical purposes. By contrast, the uncertainty on ($\mathbf{B\bar{B}}$)—where the dominant propagation mechanisms change from near-LOS to reflection, diffraction, and scattering—is relatively small for 0–6 m, but increases moving into the deeply shadowed region. The uncertainty introduced by each interaction of the propagating wave with the environment tends to accumulate over longer paths.

Of particular interest is determining which material properties contribute most toward the uncertainty in the path loss (i.e. the relative sensitivities) and can be quantified using (7) and (8). If it is possible to reduce the uncertainty in the input parameters (e.g. via additional measurements) the sensitivity analysis indicates which inputs should be targeted to have the greatest reduction in the output variability. Fig. 3(b) shows the relative contribution of each material property to the uncertainty observed on $\mathbf{B\bar{B}}$ (the sum of the Sobol indices at each point has been normalized to 1.0). In near-LOS regions (0–9 m) the path loss is most sensitive to the dielectric

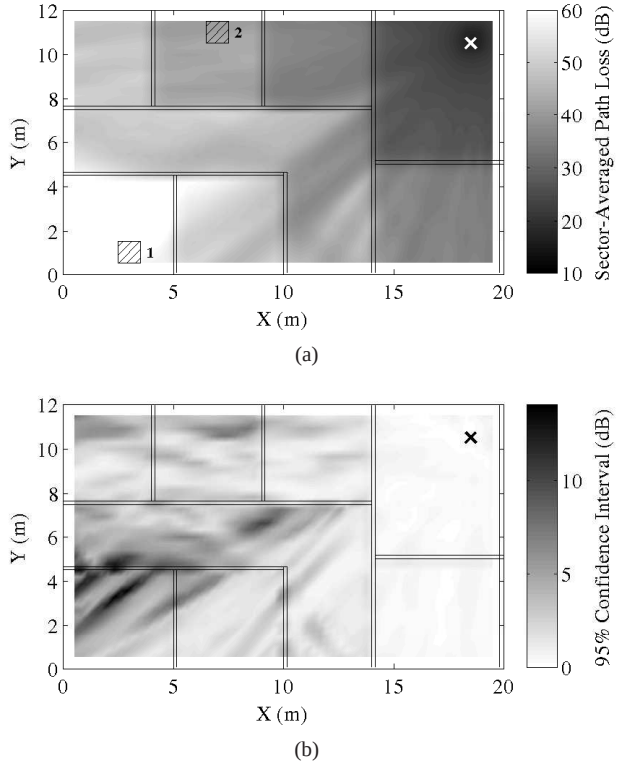

Fig. 4. Density plots of the statistics for the sector-averaged path loss when the nominal position of each internal wall is assumed to be random: (a) Mean; and (b) 95% confidence interval. The location of the sectors used to compute the PDFs are indicated.

properties of the drywall, in particular the relative permittivity. By contrast, moving into the shadowed region (9–18 m) increases the relative contribution of the glass.

B. Building Geometry Uncertainty

The 'nominal' building geometry considered in this section is shown in Fig. 4(a). The size of the computational lattice is reduced, but the other FDTD simulation parameters are kept the same as the previous section. Randomness is introduced by assuming that the spatial location of eight internal walls (in the direction normal to the wall orientation) follows a uniform distribution, with limits ± 10 cm. It is assumed that the wall thickness (0.15 m) and material properties remain constant ($\epsilon_r = 3$ and $\sigma_E = 12$ mS/m). In cases where the dielectric walls are not aligned with the FDTD lattice, effective properties for the boundary cells are computed based on the weighted average. Similar to the previous section, a set of quadrature points is generated using the Smolyak algorithm; in this case Kronrod-Patterson quadrature rules were used to reduce the computational costs. The FDTD model is solved at each quadrature point and the results collated to solve for the coefficients in the polynomial chaos expansion. For total order $D = \{2, 3\}$ the number of FDTD simulations required are 129 and 609 respectively.

Fig. 4(a) and (b) show the mean and 95% CIs for the sector-averaged path loss, computed from polynomial chaos expansions truncated at $D = 3$. Similar to the previous results, the 95% CIs are generally low (< 1 dB) in regions where

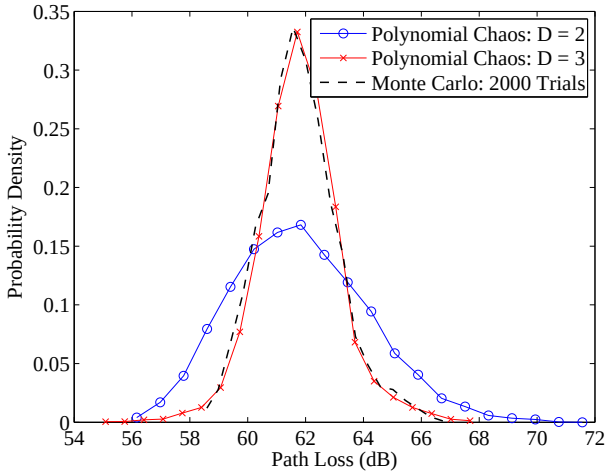

(a)

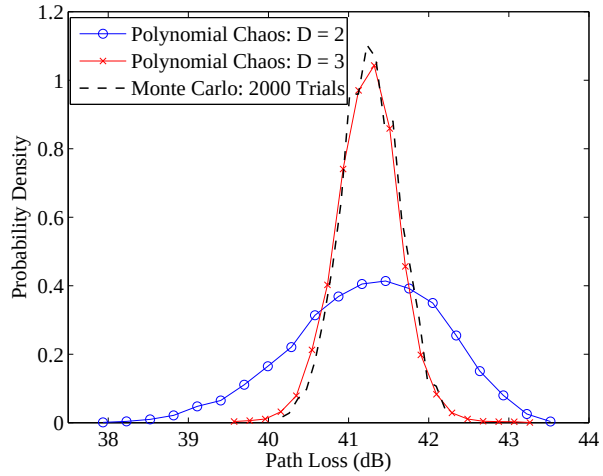

(b)

Fig. 5. Probability distributions of the path loss due to uncertainty in the building geometry—computed using polynomial chaos (order $D = \{2, 3\}$) and 2000 Monte-Carlo simulations—(a) sector 1 centred at $x = 3$ m, $y = 1$ m; and (b) sector 2 centred at $x = 7$ m, $y = 11$ m.

the LOS (or near-LOS) component dominates. The 95% CIs tends to increases with propagation through the internal walls, reaching a maximum of 14.4 dB. Uncertainty in the location of the walls introduces randomness to any wave components penetrating through or reflecting from the interface and the effect of such multiple interactions accumulates. By contrast, waves travelling over on LOS paths generally have few interactions with the environment and are thus less affected by uncertainty.

Fig. 5(a) and (b) show PDFs of the path loss computed using polynomial chaos and 2000 Monte Carlo trials. For both sectors examined, truncating the expansion at $D = 2$ predicts the mean value accurately (relative to the Monte Carlo results), however, accuracy of the higher statistical moments is significantly reduced. The statistics and PDFs computed at $D = 3$ agree more closely with the Monte Carlo simulations (similar findings can be observed for other sectors). The polynomial chaos expansion can be interpreted as an interpolation in the random parameter space, $\boldsymbol{\xi}$, and depending on the complexity of the underlying system higher (uni- and multi-variate) polynomial terms may be required to achieve convergence. These results suggest the path loss is more strongly influenced by the wall position than the material properties.

TABLE II
INPUT PARAMETERS AND UNCERTAINTY FOR RAY TRACING ANALYSIS

		Nominal Value	Distribution
Antenna Heights	h_t	2.0 m	Gaussian, $\sigma = 0.03$ m
	h_r	1.8 m	Gaussian, $\sigma = 0.03$ m
Lateral Position	L_t	3.36 m	Gaussian, $\sigma = 0.15$ m
	L_r	2.36 m	Gaussian, $\sigma = 0.15$ m
Surface Roughness	σ_h	0.0 m	Uniform, 0–0.05 m
Concrete Permittivity	ϵ_r	5.0	Gaussian, $\sigma = 0.50$

IV. UNCERTAINTY IN RAY-TRACING CHANNEL MODELS

An image-based ray-tracer [26] is used to examine radio-wave propagation in a ground-floor parking garage at 2.4 GHz. The environment is electrically large and has been previously used to test and calibrate equipment prior to deployment in railway tunnels. The ray-tracing results are compared against a site-survey conducted when the garage was empty. The goal of the uncertainty analysis is to estimate the variability in the simulated received power due to uncertainty in the environment and experimental setup. Table II lists the uncertain inputs parameters considered. The uncertainties in the height and lateral separation account for random error introduced when positioning equipment during the site-survey, and are assumed to follow Gaussian distributions.

The floor and ceiling are formed from poured concrete, and surface roughness is included by altering the reflection coefficients to account for diffuse reflection [27, pp. 16–17]. Partial side walls, concrete pillars and overhangs complicate the analysis, but as these are relatively small the effects tend to be localized and have been ignored in this study. Directional antennas were used at both the transmitter and receiver, and the measured radiation patterns embedded in the ray-tracer. Increasing the number of reflections improves the results, but adds considerably to computational costs; for this analysis the maximum number of interactions was restricted to six, which provided an adequate trade-off between accuracy and speed.

Fig. 6(a) shows the uncertainty in the ray-tracing predictions of the received power as a function of the transmitter-receiver separation distance. The mean and 90% confidence intervals are computed using a polynomial chaos expansion truncated at $D = 2$, with Smolyak sparse grids formed from Kronrod-Patterson quadrature rules. In total, 73 simulations were required. Also shown are the same statistics computed using 2000 Monte-Carlo simulations; the close agreement demonstrates the validity of the polynomial chaos approach. The received power increases initially as the transmitter and receiver are offset in the horizontal (lateral) direction by 1.0 m, and consequently the LOS component is outside the main

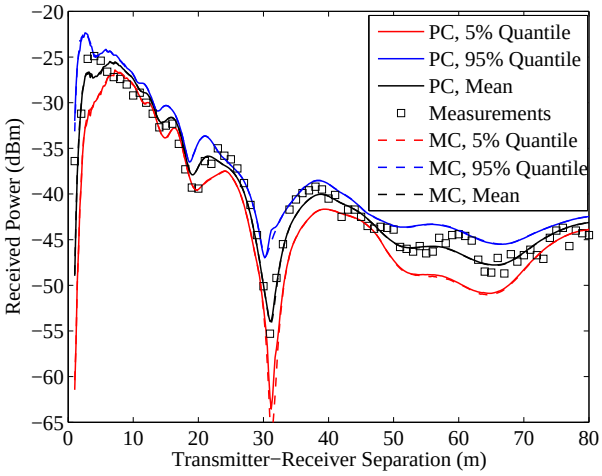

(a)

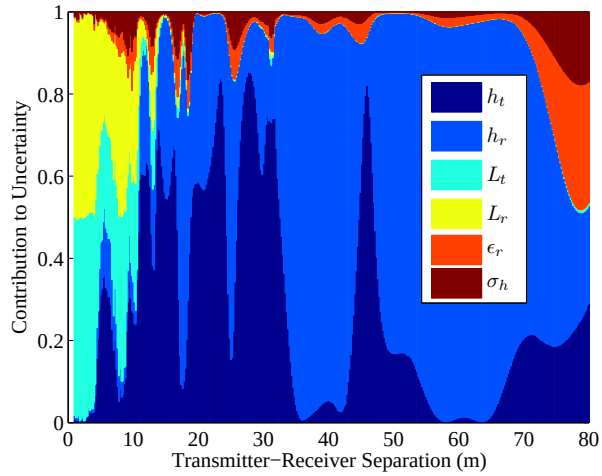

(b)

Fig. 6. Ray-tracing results for 2.4 GHz propagation in a ground-floor garage. (a) Statistics of the received power versus distance—computed using the polynomial chaos expansion (PC) and 2000 Monte-Carlo trials (MC)—compared against experimental measurements; and (b) Relative contribution of each input parameter to the uncertainty in the received power as a function of distance.

beam of either the transmitting or receiving antenna. This effect is also captured in the experimental measurements.

Randomness in the transmitter and receiver position alters the length (and thus the relative phase) of the reflected propagation paths. This leads to constructive or destructive interference at the receiver, thereby introducing uncertainty in the predictions of the power. Similarly, randomness in the permittivity and surface roughness introduces uncertainty in the magnitude and phase of the reflected components. It is also noted that although the input uncertainties are small, the spread in the predicted power is relatively large. For example, at a transmitter-receiver separation of 31 m the mean received power is -53 dBm, however the spread is large and asymmetric, with 90% of the data falling between -45 dBm and -65 dBm.

Fig. 6(b) shows the relative contribution each input parameter makes toward the total uncertainty as a function of distance, computed using (8). For small separation distances (1–10 m) the uncertainty in the lateral positions of the transmitting and receiving antennas dominates. This is expected as propagation in this region is largely governed by the LOS path. In general, beyond 10 m separation, uncertainties in the heights of both transmitting and receiving antennas introduce most of the uncertainty in the received power. For example, the largest uncertainty occurs at 31 m separation and is almost entirely caused by the randomness in the height of the transmitting antenna. Results also indicate uncertainty in the surface roughness and permittivity have little effect—the increase in the relative contribution of ϵ_r and σ_h beyond 70 m occurs in region where the overall uncertainty in the path loss is low. As the separation distance increases, the angle of incidence for most reflected rays approaches glancing, i.e. the reflection coefficients tend toward -1. Thus, the relative strength of reflected components becomes independent of the material properties. The measured data generally follows the ray-tracing results, with most points falling within the 90% CI. However, the deviation from the ray-tracing results at some locations suggests not all the variation can be associated with the uncertainty in the input parameters. Other features of the channel, such as local scattering from objects in the environment may be required to improve the predictions.

V. Conclusions

Most previous applications of deterministic channel models to characterize indoor propagation assume nominal (and constant) values for the input parameters such as dielectric properties, geometry and antenna positions. In many cases these parameters are not well defined and must be considered random, i.e. a degree of uncertainty exists. This input uncertainty will 'propagate' through the deterministic models to introduce uncertainty in the predictions. The results presented in this paper show that for typical parameter variations the uncertainty in the modelled path loss can be large (in some cases greater than 10 dB) and thus cannot be ignored when applying deterministic channel models to plan system deployments. Although the levels of uncertainty are specific to the problem, the size of the 95% confidence intervals is generally observed to increase with distance. Non-intrusive polynomial chaos provides a method to accurately characterize these uncertainties at significantly lower computational cost than competing methods.

Appendix A
Polynomial Chaos Basis in Multiple Variables

The polynomial chaos basis is a multi-variate function of the N input variables, $\boldsymbol{\xi} = \{\xi_1, \xi_2, \ldots \xi_N\}$, and can be expressed

$$\Psi_j(\boldsymbol{\xi}) = \prod_{i=1}^{N} \phi_{m_i^j}(\xi_i), \tag{9}$$

where $\phi_{m_i^j}(\xi_i)$ is a one-dimensional orthogonal polynomial in ξ_i, m_i^j is the multi-index corresponding to the order, and $j = 0 \ldots P$. While any suitable orthogonal functions may

be used, it can be shown that the optimal polynomial basis, $\phi(\xi_i)$, depends on the distribution of random variable ξ_i [16]. This association is termed the Weiner-Askey scheme—in which, Gaussian distributed inputs are associated with Hermite polynomials and uniformly distributed inputs with Legendre polynomials [16]. For example, the polynomial chaos basis functions truncated at total order $D = 3$, for $N = 2$ (where ξ_1 is Gaussian distributed, and ξ_2 is uniformly distributed) are

$$\begin{aligned}
\Psi_0(\boldsymbol{\xi}) &= \phi_0(\xi_1)\phi_0(\xi_2) = 1 \\
\Psi_1(\boldsymbol{\xi}) &= \phi_0(\xi_1)\phi_1(\xi_2) = \xi_2 \\
\Psi_2(\boldsymbol{\xi}) &= \phi_1(\xi_1)\phi_0(\xi_2) = \xi_1 \\
\Psi_3(\boldsymbol{\xi}) &= \phi_1(\xi_1)\phi_1(\xi_2) = \xi_1\xi_2 \\
\Psi_4(\boldsymbol{\xi}) &= \phi_0(\xi_1)\phi_2(\xi_2) = \frac{1}{2}(3\xi_2^2 - 1) \\
\Psi_5(\boldsymbol{\xi}) &= \phi_2(\xi_1)\phi_0(\xi_2) = \xi_1^2 - 1 \\
\Psi_6(\boldsymbol{\xi}) &= \phi_1(\xi_1)\phi_2(\xi_2) = \frac{1}{2}\xi_1(3\xi_2^2 - 1) \\
\Psi_7(\boldsymbol{\xi}) &= \phi_2(\xi_1)\phi_1(\xi_2) = (\xi_1^2 - 1)\xi_2 \\
\Psi_8(\boldsymbol{\xi}) &= \phi_0(\xi_1)\phi_3(\xi_2) = \frac{1}{2}(5\xi_2^3 - 3\xi_2) \\
\Psi_9(\boldsymbol{\xi}) &= \phi_3(\xi_1)\phi_0(\xi_2) = \xi_2^3 - 3\xi_2.
\end{aligned}$$

APPENDIX B
SMOLYAK SPARSE GRIDS

The Smolyak algorithm selectively combines the tensor-products of lower order quadrature rules to more efficiently cover the parameter space for low-order terms. For N dimensions, with maximum order d, the Smolyak approximation to (4) is given by [20]

$$U = \sum_{d-N+1 \le |\mathbf{i}| \le d} (-1)^{d-|\mathbf{i}|} \binom{N-1}{d-|\mathbf{i}|} (Q_{i_1} \otimes \ldots \otimes Q_{i_N}) \tag{10}$$

where $\{Q_{i_1}, \ldots Q_{i_N}\}$ are one-dimensional quadrature rules for the N inputs, and $\mathbf{i}$ represents the orders that are combined. The Smolyak algorithm in (10) can be applied to any set of suitable one-dimensional quadrature rules, however, sparse grids formed from nested integration rules are also interpolatory. Nested rules, such as Kronrod-Patterson, retain quadrature points as the order of integration increases. These consequently introduce less error than non-nested rules if the order of the integrand exceeds that of the quadrature rule [28].

REFERENCES

[1] M. J. Neve, K. W. Sowerby, A. G. Williamson, G. B. Rowe, J. C. Batchelor, and E. A. Parker, "Physical layer engineering for indoor wireless systems in the Twenty-First century," in *Proc. Loughborough Antennas Propag. Conf.*, 2010, pp. 72–78.

[2] S. Y. Seidel and T. S. Rappaport, "Site-specific propagation prediction for wireless in-building personal communication system design," *IEEE Trans. Veh. Technol.*, vol. 43, no. 4, pp. 879–891, Nov. 1994.

[3] G. E. Athanasiadou and A. R. Nix, "A novel 3-D indoor ray-tracing propagation model: The path generator and evaluation of narrow-band and wide-band predictions," *IEEE Trans. Veh. Technol.*, vol. 49, no. 4, pp. 1152–1168, July 2000.

[4] A. Alighanbari and C. D. Sarris, "Rigorous and efficient time-domain modeling of electromagnetic wave propagation and fading statistics in indoor wireless channels," *IEEE Trans. Antennas Propag.*, vol. 55, no. 8, pp. 2373–2381, Aug. 2007.

[5] ——, "Parallel time-domain full-wave analysis and system-level modeling of ultrawideband indoor communication systems," *IEEE Trans. Antennas Propag.*, vol. 57, no. 1, pp. 231–240, Jan. 2009.

[6] A. C. M. Austin, M. J. Neve, G. B. Rowe, and R. J. Pirkl, "Modeling the effects of nearby buildings on inter-floor radio-wave propagation," *IEEE Trans. Antennas Propag.*, vol. 57, no. 7, pp. 2155–2161, July 2009.

[7] A. C. M. Austin, M. J. Neve, and G. B. Rowe, "Modeling propagation in multifloor buildings using the FDTD method," *IEEE Trans. Antennas Propag.*, vol. 59, no. 11, pp. 4239–4246, 2011.

[8] A. Safaai-Jazi, S. M. Riad, A. Muqaibel, and A. Bayram, "Through-the-wall propagation and material characterization," Virginia Polytechnic Institute and State University, Tech. Rep., 2002.

[9] Recom. ITU-R P.1238-6, "Propagation data and prediction methods for the planning of indoor radiocommunication systems and radio local area networks in the frequency range 900 MHz to 100 GHz," 2009.

[10] R. G. Ghanem and P. D. Spanos, *Stochastic Finite Elements: A Spectral Approach*. New York: Springer-Verlag, 1991.

[11] O. P. Le Maître and O. M. Knio, *Spectral Methods for Uncertainty Quantification With Applications to Computational Fluid Dynamics*. Heidelberg: Springer-Verlag, 2010.

[12] S. Wang and J. Reed, "Analysis of parameter sensitivity in a ray-tracing propagation environment," in *Proc. IEEE Veh. Technol. Soc. Conf.*, vol. 2, May 1997, pp. 805–809.

[13] G. E. Athanasiadou and A. R. Nix, "Investigation into the sensitivity of the power predictions of a microcellular ray tracing propagation model," *IEEE Trans. Veh. Technol.*, vol. 49, no. 4, pp. 1140–1151, July 2000.

[14] F. Hastings, J. Schneider, and S. Broschat, "A Monte-Carlo FDTD technique for rough surface scattering," *IEEE Trans. Antennas Propag.*, vol. 43, no. 11, pp. 1183–1191, 1995.

[15] N. Wiener, "The homogeneous chaos," *Amer. J. Math.*, vol. 60, pp. 897–936, 1938.

[16] D. Xiu and G. Karniadakis, "The Wiener-Askey polynomial chaos for stochastic differential equations," *SIAM J. Sci. Comput.*, vol. 24, no. 2, pp. 619–644, 2002.

[17] R. S. Edwards, A. C. Marvin, and S. J. Porter, "Uncertainty analyses in the finite-difference time-domain method," *IEEE Trans. Electromagn. Compat.*, vol. 52, no. 1, pp. 155–163, Feb. 2010.

[18] J. Silly-Carette, D. Lautru, M.-F. Wong, A. Gati, J. Wiart, and V. Fouad Hanna, "Variability on the propagation of a plane wave using stochastic collocation methods in a bio electromagnetic application," *IEEE Microw. Wireless Compon. Lett.*, vol. 19, no. 4, pp. 185–187, 2009.

[19] O. Aiouaz, D. Lautru, M.-F. Wong, E. Conil, A. Gati, J. Wiart, and V. F. Hanna, "Uncertainty analysis of the specific absorption rate induced in a phantom using a stochastic spectral collocation method," *Ann. Telecommun.*, vol. 66, no. 7–8, pp. 409–418, 2011.

[20] D. Xiu, "Efficient collocational approach for parameteric uncertainty analysis," *Commun. Comput. Phys.*, vol. 2, no. 2, pp. 293–309, 2007.

[21] M. Abramowitz and I. A. Stegun, Eds., *Handbook of Mathematical Functions with Formulas, Graphs, and Mathematical Tables*, 9th ed. New York: Dover Publications Inc., 1972.

[22] F. Heiss and V. Winschel, "Likelihood approximation by numerical integration on sparse grids," *J. Econometrics*, vol. 144, pp. 62–80, 2008.

[23] T. Crestaux, O. Le Maitre, and J.-M. Martinez, "Polynomial chaos expansion for sensitivity analysis," *Reliab. Eng. Syst. Safe.*, vol. 94, no. 7, pp. 1161–1172, 2009.

[24] A. Taflove and S. C. Hagness, *Computational Electrodynamics: The Finite-Difference Time-Domain Method*, 3rd ed. Boston: Artech House, 2005.

[25] R. A. Valenzuela, O. Landron, and D. L. Jacobs, "Estimating local mean signal strength of indoor multipath propagation," *IEEE Trans. Veh. Technol.*, vol. 46, no. 1, pp. 203–212, 1997.

[26] N. Sood, L. Liang, S. V. Hum, and C. D. Sarris, "Ray-tracing based modeling of ultra-wideband pulse propagation in railway tunnels," in *Proc. IEEE APS/URSI Int. Symp.*, July 2011, pp. 2383–2386.

[27] M. F. Catedra and J. Perez-Arriaga, *Cell Planning for Wireless Communications*. Boston: Artech House, 1999.

[28] T. Gerstner and M. Griebel, "Numerical integration using sparse grids," *Numerical Algorithms*, vol. 18, pp. 209–232, 1998.

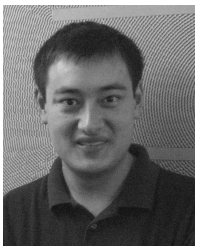

Andrew C. M. Austin received the B.E. (Hons.) and Ph.D. degrees in electrical and electronic engineering from the University of Auckland, Auckland, New Zealand, in 2007 and 2011, respectively.

He is currently a Postdoctoral Fellow in the Edward S. Rogers Sr. Department of Electrical and Computer Engineering at the University of Toronto, Toronto, ON, Canada. His research interests include radiowave propagation modelling, computational electromagnetics and uncertainty analysis.

Dr. Austin was awarded a New Zealand Tertiary Education Commission Bright Futures Top Achiever Doctoral Scholarship in 2007.

Neeraj Sood was born in Punjab, India, in 1986. He received the B.A.Sc degree in Electrical Engineering from the University of Toronto in 2009. He did a 16 month internship with Altera Corporation during his B.A.Sc where he worked with the Timing Modeling group. He received the M.A.Sc degree in Electrical Engineering from the University of Toronto in 2012.

He is currently pursuing a Ph.D. in Electrical Engineering from the University of Toronto. His current research interests include computational electromagnetics, wireless channel modeling and ray-tracing.

Mr. Sood is a student member of the Institute of Electrical and Electronics Engineers (IEEE).

Joseph Siu holds a Masters of Engineering degree (M.Eng.) and B.A.Sc. degree in Engineering Science from University of Toronto.

He has been working in the field of urban train control communication system for the last 10 years, and had been a key contributor to the design of Thales' data communication system (DCS) for communication based train control. He was the DCS technical lead for over 8 projects, and is currently responsible for DCS platform management.

Costas D. Sarris received the Ph.D. degree in electrical engineering and M.Sc. degree in applied mathematics from the University of Michigan, Ann Arbor, in 2002.

He is currently a Full Professor and the Eugene V. Polistuk Chair in Electromagnetic Design at the Department of Electrical and Computer Engineering and an Associate Chair of the Division of Engineering Science, University of Toronto, Toronto, ON, Canada. His research interests are in the area of numerical electromagnetics, with emphasis on high-order, multiscale/multi-physics computational methods, modeling under stochastic uncertainty, as well as applications of numerical methods to wireless channel modeling, wave-propagation in complex media and metamaterials, biomedical imaging and hyperthermia, wireless power transfer and electromagnetic compatibility/interference (EMI/EMC) problems.

Prof. Sarris was the recipient of the IEEE MTT-S Outstanding Young Engineer Award in 2013 and an Early Researcher Award from the Ontario Government in 2007. His students have received paper awards at the 2009 IEEE MTT-S International Microwave Symposium, the 2008 Applied Computational Electromagnetics Society Conference, and the 2008 and 2009 IEEE International Symposia on Antennas and Propagation. He currently serves as an associate editor for the IEEE TRANSACTIONS ON MICROWAVE THEORY AND TECHNIQUES. He was the Technical Program Committee Vice-Chair for the 2012 IEEE MTT-S International Microwave Symposium, an Area Editor (Numerical Modeling) for the IEEE Microwave Magazine and an Associate Editor for the IEEE MICROWAVE AND WIRELESS COMPONENTS LETTERS.